Biosensors and Bioelectronics 46 (2013) 74–79

Contents lists available at SciVerse ScienceDirect

Biosensors and Bioelectronics

journal homepage: www.elsevier.com/locate/bios

# Multi-labeled functionalized $C_{60}$ nanohybrid as tracing tag for ultrasensitive electrochemical aptasensing

Jing Han [a], Ying Zhuo [a,*], Yaqin Chai [a], Ruo Yuan [a,*], Yun Xiang [a], Qiang Zhu [a,b], Ni Liao [a]

[a] Education Ministry Key Laboratory on Luminescence and Real-Time Analysis, College of Chemistry and Chemical Engineering, Southwest University, Chongqing 400715, China

[b] College of Chemistry, Chongqing Normal University, Chongqing 400047, China

ARTICLE INFO

*Article history:*
Received 18 November 2012
Received in revised form
25 January 2013
Accepted 12 February 2013
Available online 24 February 2013

*Keywords:*
Functionalized $C_{60}$ nanoparticles
Supramolecular interaction
Dual signal amplification
Aptasensor

ABSTRACT

This work reports a new supramolecular method for the synthesis of the amino and thiol groups functionalized $C_{60}$ nanoparticles ($FC_{60}$NPs) with the large surface active sites and good water solubility. First, Prussian blue carried gold nanoparticles were decorated onto the surface of the obtained $FC_{60}$NPs (abbreviated as Au@PB/$FC_{60}$). Subsequently, the Au@PB/$FC_{60}$ was labeled by detection aptamers and alkaline phosphatase to act as tracer. On the other hand, onion-like mesoporous graphene sheets and gold nanoparticles were utilized as the biosensor platform to immobilize a large amount of capture aptamers, owing to theirs porous structure and high surface-to-volume ratio. Based on the sandwich format, a dual signal amplification strategy based on multi-labeled functionalized $C_{60}$ nanohybrid as tracing tag has been successfully developed for platelet-derived growth factor B-chain electrochemical detection with a wide linear response in the range of 0.002–40 nM and a limit of detection of 0.6 pM ($S/N=3$). The proposed aptasensor demonstrated good specificity and high sensitivity, implying potential applications in bioanalysis and biomedicine.



## 1. Introduction

$C_{60}$, a kind of fullerene, has been investigated extensively since 1985 (Kroto et al., 1985). Nowadays, $C_{60}$ derivatives are still extensively studied because of its notable electronic properties and the possibility to perform precise chemical modification, which prompt such materials to have potential applications in various physical, chemical and biomedical fields (Martín, 2006; Regehly et al., 2007; Xu et al., 2011). The pristine $C_{60}$ nanoparticles (*nano*-$C_{60}$) could be obtained by simply stirring or ultrasonication treatments (Andrievsky et al., 1999; Ko et al., 2004). However, the obtained *nano*-$C_{60}$ was not desirable candidates for biomedical applications in aqueous and biological systems because their aggregation behavior and the trend to be released into natural waters (Mashayekhi et al., 2012). To overcome these limitations, the researchers devoted to the covalent binding of *nano*-$C_{60}$ to amino acids, hydroxyl groups, carboxyl groups etc., which can increase the nanoparticles' ability to interact with the biological environment (Colvin, 2003; Yang and Barron, 2004; Zhong et al., 2012). Although these methods have proven useful, they still have significant limitations that may change the original structure and properties of the $C_{60}$, such as the physical, electrical and mechanical properties. Supramolecular chemistry, the chemistry of the intermolecular bond, aims at developing highly complex chemical system components in interacting by non-covalent intermolecular forces. The non-covalent interaction for the synthesis of functionalized $C_{60}$ based on supramolecular chemistry would preserve the original structure and integral electrochemical characteristics of $C_{60}$, which was superior to the traditional covalently bonded methods. Therefore, non-covalent interaction for the synthesis of $C_{60}$-based rich conjugated $\pi$ electron compounds (such as porphyrin (Poddutoori et al., 2010), phthalocyanine (Pereira et al., 2012), tetrathiafulvalene (Nielsen et al., 2006), perylene (D'Souza and Ito, 2009)) and macrocyclic molecules (such as cyclodextrin (Liu et al., 2006), arene (Halder et al., 2012), azacalix (Zhang et al., 2008)) through supramolecular chemistry have been recently investigated. As a kind of $\pi$ electron compounds, the amino functionalized 3,4,9,

*Abbreviations:* ($C_{60}$), Fullerene; (*nano*-$C_{60}$), Pristine $C_{60}$ nanoparticles; (PTC-$NH_2$), Amino functionalized 3,4,9,10-perylenetetracarboxylic dianhydride; (PTC–$NH_2$–$C_{60}$), Amido functionalized *nano*-$C_{60}$; ($FC_{60}$NPs), Amino and thiol groups functionalized $C_{60}$ nanoparticles; (Au@PBNPs), Prussian blue carried gold nanoparticles; (abbreviated as Au@PB/$FC_{60}$), Combination of Au@PBNPs and the $FC_{60}$NPs; (O-GS), Onion-like mesoporous graphene sheets; (PDGF-BB), Platelet-derived growth factor B-chain; (Apt I), Capture aptamers; (Apt II), Detection aptamers; (AP), Alkaline phosphatase; (AA–P), Ascorbic acid 2-phosphate; (DHA), Dehydroascorbic acid

* Corresponding authors at: Southwest University, College of Chemistry and Chemical Engineering, Education Ministry Key Laboratory on Luminescence and Real-Time Analysis, No. 2 Tiansheng Road, BeiBei District, Chongqing 400715, China. Tel.: +86 23 68252277; fax: +86 23 68253172.

*E-mail addresses:* yingzhuo@swu.edu.cn (Y. Zhuo), yuanruo@swu.edu.cn (R. Yuan).

0956-5663/$ - see front matter © 2013 Elsevier B.V. All rights reserved.
http://dx.doi.org/10.1016/j.bios.2013.02.020

10-perylenetetracarboxylic dianhydride (PTC–$NH_2$) was shown ideal characteristics for the electrode surface modification, owing to its porous structure, desirable organic electronic and optical properties in our previous studies (Li et al., 2010; Zhuo et al., 2008). More importantly, we found that PTC–$NH_2$ could be bond to the surface of *nano*-$C_{60}$ *via* supramolecular interaction due to the planar $\pi$ surfaces and benzene ring structure of PTC–$NH_2$ to obtain the functionalized $C_{60}$ nanoparticles ($FC_{60}$NPs) with the good water-stability and increasing the surface active sites.

With the development of nanotechnology, various types of nanomaterials have been applied as the labels in nanomaterials-based amplification platforms which can dramatically amplify the response of electrochemical biosensor and lead to ultrasensitive bioassays (Lei and Ju, 2012; Lin et al., 2012; Zhou et al., 2012). Prussian blue carried gold nanoparticles (Au@PBNPs), which possessed excellent electrochemical activity, redox biocompatibility and sensing activities, have been generally investigated for the amplification of the electrochemical signal by the previous report (Qiu et al., 2007; Zhuo et al., 2009). Herein, Au@PBNPs were decorated onto the surface of the obtained $FC_{60}$NPs *via* covalent bond. The combination of Au@PBNPs and the $FC_{60}$NPs (abbreviated as Au@PB/$FC_{60}$) possesses the high electrocatalytic activity and high-performance amperometric response, therefore, is very important for probe construction.

Platelet-derived growth factor B-chain (PDGF-BB), a cancer-related protein, is known to be related to tumor growth, transformation and progression (Doolittle et al., 1983; Huang et al., 2005). Therefore, precise and sensitive evaluation of PDGF-BB in biological samples could help early diagnosis, treatment, and prognosis of cancers. Herein, using PDGF-BB as a model target, we employed Au@PB/$FC_{60}$ as tracing tag to label the detection aptamers (Apt II) and couple with alkaline phosphatase (AP) for electrochemical aptasensing. The dual signal amplification strategy can be achieved by biocatalysis of AP towards ascorbic acid 2-phosphate (AA–P) to in-situ production of AA and then chemicatalysis of Au@PB/$FC_{60}$ towards AA to generate dehydroascorbic acid (DHA). On the other hand, in recent years, graphene sheets (GS) has been extensively studied in many technological fields such as catalysis, nanocomposites and nanoelectronics (Guo et al., 2011; Machado and Serp, 2012; Park and Ruoff, 2009; Stankovich et al., 2006). Superior to GS, the onion-like mesoporous graphene sheets (O-GS) is a novel kind of excellent nanomaterial, which possessed onion-like lamellar structure and favorable electrical properties. Thus, we utilized O-GS and AuNPs as the biosensor platform to immobilize a large amount of capture aptamers (Apt I) due to theirs favorable microenvironment and the enhancing surface area. Meanwhile, the performance characteristics of the proposed aptasensor and potential merits for PDGF-BB detection were presented in detail.

## 2. Experimental

### 2.1. Reagent and materials

Fullerene ($C_{60}$) and onion-like mesoporous graphene sheets (O-GS) were obtained in Pioneer Nanotechnology Co. (Nanjing, China). Alkaline phosphatase (AP) was purchased from Promega (USA). Platelet-derived growth factor B-chain (PDGF-BB), ascorbic acid 2-phosphate (AA–P), hexanethiol (96%, HT), bovine serum albumin (BSA), L-cysteine (Cys) and gold chloride ($HAuCl_4$) were obtained from Sigma Chemical Co. (St. Louis, MO, USA). 3,4,9, 10-perylenete-tracarboxylic dianhydride ($C_{24}H_8O_6$, PTCDA) was purchased from Lian Gang Dyestuff Chemical Industry Co. Ltd (Liaoning, China). Cetyltrimethylammonium bromide (CTAB) was purchased from Chemical Reagent Co. (Sichuan, China). The colloidal AuNPs of 16 nm diameter (the graph not shown) were prepared by reducing $HAuCl_4$ with sodium citrate at 100 °C for half an hour (Enustun and Turkevich, 1963). The PDGF-BB binding aptamer (PBA) was ordered from Takara Biotechnology Co., Ltd. (Dalian, China) with the sequence as follows:

PBA: 5′-$NH_2$-$(CH_2)_6$-CAGGCTACGGCACGTAGAGCATCAC CATGATCCTG-3′

0.1 M phosphate buffered solutions (PBS) containing 10 mM KCl and 2 mM $MgCl_2$ (pH 6.86) was employed to investigate the performance of electrodes. 20 mM Tris–HCl buffer (pH 7.4) containing 140 mM NaCl, 5 mM KCl and 1 mM $MgCl_2$ was used to prepare aptamer solutions. Ultrapure water was used throughout this study.

### 2.2. Apparatus

Cyclic voltammetry (CV) and differential pulse voltammetry (DPV) measurements were carried out with a CHI 660D electrochemical workstation (Shanghai Chen Hua Instrument, Co., China). A three-electrode electrochemical system contained a platinum wire auxiliary electrode, a saturated calomel reference electrode (SCE) and the modified glassy carbon electrode (GCE, $\Phi$=4 mm) as the working electrode. All potentials were measured and reported versus the SCE. The scanning electron micrographs were taken with a scanning electron microscope (SEM, S-4800, Hitachi, Japan) at an acceleration voltage of 14 kV. The sizes of nanoparticles were measured by transmission electron microscopy (TEM, Hitachi 600, Japan) at an operating voltage of 80 kV. The pH measurements were made with a pH meter (MP 230, Mettler-Toledo Switzerland) and a digital ion analyzer (Model PHS-3C, Dazhong Instruments, Shanghai, China).

### 2.3. Preparation of the $FC_{60}$NPs

The synthesis was performed in the following manner. The first step: 0.01 g PTCDA was dissolved in 2 mL of ethanol under stirring, and then 20 μL anhydrous ethylenediamine was dropped gradually into above solution at 4 °C. After stirring for 2 h, the product of PTC–$NH_2$ was centrifuged and washed extensively with acetone and ethanol. The resulted product was finally kept in a vacuum at room temperature for drying. Moreover, the *nano*-$C_{60}$ suspension was prepared by solvent-exchange method according to the literature (Hilburn et al., 2012). The second step: 1 mg PTC–$NH_2$ was dispersed in 1 mL of the prepared *nano*-$C_{60}$ suspension with an ultrasonic bath for about 2 h to obtain the amido functionalized *nano*-$C_{60}$ (PTC–$NH_2$–$C_{60}$) *via* supramolecular chemistry. The obtained product was washed three times by ultrapure water and collected by centrifugation. The third step: In order to increase active groups of PTC–$NH_2$–$C_{60}$, the Cys solution was first activated by the aid of EDC and NHS, and then PTC–$NH_2$–$C_{60}$ was added and the resultant mixture was allowed to react overnight under vigorously stirring to produce $FC_{60}$NPs with the amino groups and thiol groups. After centrifugation at 12,000 rpm for 15 min to remove surplus Cys, the sediment of $FC_{60}$NPs were resuspended in ultrapure water and stored at 4 °C for further use.

### 2.4. Preparation of Au@PBNPs

The Au@PBNPs were prepared in the following procedure: Initially, 10 mL of 0.01 M $FeCl_3$ containing a slight excessive $H_2O_2$ was dropped gradually into 10 mL of 0.01 M $K_3[Fe(CN)_6]$ containing 0.1 mM HCl under ultrasonic condition (Fiorito et al., 2005; Liu et al., 2002). Following that, the resultant mixture was continuously stirred for about 0.5 h and separated by

centrifugation and washed with ultrapure water several times to obtain PBNPs. Subsequently, the product of PBNPs were dissolved in 25 mL of 1 mg/mL BSA under vigorous stirring to obtain BSA-coated PBNPs, and then centrifuged and washed with ultrapure water to remove excess reagents. Ultimately, BSA-coated PBNPs were dispersed in 10 mL of as-prepared colloidal AuNPs for 4 h to obtain Au@PBNPs which were centrifuged, washed and finally dispersed in Tris–HCl buffer.

### 2.5. Preparation of Apt II bioconjugates (AP/Apt II/Au@PB/$FC_{60}$)

The Apt II bioconjugates (AP/Apt II/Au@PB/$FC_{60}$) were prepared by the following process: Initially, 0.5 mL $FC_{60}$NPs was added into 1 mL Au@PBNPs solution with continuous stirring for 8 h to produce Au@PB/$FC_{60}$ through amino-Au affinity. Next, it was centrifuged for 15 min at 10,000 rpm and then washed and redispersed in ultrapure water. Subsequently, 100 μL PBA (2 mM) was added to 1 mL of prepared Au@PB/$FC_{60}$ followed by incubation at 4 °C for 12 h under gently stirring. Finally, 80 μL AP (0.5 mg/mL) was added into the Au@PB/$FC_{60}$ labeled PBA and incubated at 4 °C for 4 h. After centrifugation and washing, the obtained Apt II bioconjugates were resuspended in 300 μL Tris–HCl buffer. It was stable for about 14 days at 4 °C.

### 2.6. Fabrication of the aptasensor

Prior to use, 1 mg O-GS was dispersed in 1 mL CTAB aqueous solution (1 wt%) with the aid of ultrasonication for 2 h (Note: CTAB is a cationic surfactant). Next, the pretreated GCE was coated with 10 μL the obtained O-GS suspension and dried in the air. Following that, the O-GS modified electrode was immersed into 2 mL colloidal AuNPs for 4 h to obtain the AuNPs/O-GS/GCE *via* electrostatic interaction between the positively charged O-GS and the negatively charged AuNPs. Subsequently, the AuNPs/O-GS modified electrode was submerged into 2 mM PBA for 16 h to immobilize the Apt I *via* amino-Au affinity. Afterward, the resulting electrode was incubated with 1.0 mM HT for 1 h to block nonspecific binding sites. After every step, the modified electrode was extensively rinsed with ultrapure water to prevent the physically absorbed species. The finished aptasensor were stored at 4 °C when not in use.

Based on the sandwich format, the prepared aptasensor were first incubated with 20 μL PDGF-BB standard solution with different concentrations for 1 h at room temperature, and then immersed into the AP/Apt II/Au@PB/$FC_{60}$ bioconjugates for another 1 h. After rinsing extensively to remove the unbounded Apt II labels, the electrode was ready for measurement. The detailed process of the signal amplification strategy can be expressed as follows: First, the AP on the AP/Apt II/Au@PB/$FC_{60}$ bioconjugates could catalyze the hydrolysis of AA–P substrate to in-situ produce AA. Subsequently, the signal was further amplified by electrochemical oxidation of the in-situ-produced AA because of the catalysis of Au@PB/$FC_{60}$. Schematic illustration of the stepwise aptasensor fabrication process and the dual signal amplification mechanism were depicted in Fig. 1.

## 3. Results and discussion

### 3.1. SEM characterizing of O-GS and AuNPs/O-GS composite membrane

The surface images of the O-GS and AuNPs/O-GS composite membrane were investigated by SEM (Fig. 2). In Fig. 2a, The SEM of O-GS presented the onion-like lamellar structure, the pore size distribution and large pore volume as well as porous structure. After AuNPs loading, many bright dots can be observed (Fig. 2b), indicating the successful adsorption AuNPs on the surface of O-GS through electrostatic interaction.

### 3.2. TEM characterizing of $FC_{60}$NPs, Au@PBNPs and Au@PB/$FC_{60}$

TEM images give the size and morphology of the as synthesized samples, as shown in Fig. 3. Fig. 3a showed the image of $FC_{60}$NPs, its morphology is somewhat irregularly shaped with the homogeneous distribution. From Fig. 3b, we can found that the large amount of AuNPs were adsorbed on the amino groups functionalized PBNPs surfaces and the average size of Au@PBNPs was about 200–300 nm. The Au@PB/$FC_{60}$ was presented in Fig. 3c, it can be seen that some of Au@PBNPs were adsorbed uniformly and tightly on the $FC_{60}$NPs around, which is different from the sole Au@PBNPs, indicating that Au@PB/$FC_{60}$ has been synthesized as expected.

### 3.3. CV characterization of aptasensor

Electrochemical characteristics of the proposed aptasensor was investigated by CV. Fig. 4A showed CVs of different modified electrodes in 5.0 mM $K_3Fe(CN)_6$ solution containing 0.1 M KCl at a scan rate of 50 mV/s. The curve (*a*) exhibited a well-defined redox wave, corresponding to the reversible redox reaction of ferricyanide ions on the bare GCE. With the immobilization of O-GS on the electrode (Fig. 4A, curve *b*), the redox peak current was increased obviously as the O-GS film could enhance the effective electrochemical surface area to facilitate the electron transfer. When the AuNPs were adsorbed on O-GS membrane, the redox peak current was further improved (Fig. 4A, curve *c*). The reason may be that the AuNPs is similar to a conducting wire, making the electron transfer easier. However, the peak current decreased clearly after PBA I was assembled on the AuNPs/O-GS/GCE (Fig. 4A, curve *d*), which ascribed to the fact that the capture aptamer can severely hinder the electron transfer of redox probe. Later on, when the non-electroactive HT was employed to block nonspecific sites, the peak current further decreased (Fig. 4A, curve *e*). Finally, the aptasensor incubated with 10 nM PDGF-BB, the CV response continued to decrease owing to the fact that the complementary pairing of PDGF-BB and PBA I retard the electron transfer tunnel (Fig. 4A, curve *f*).

### 3.4. Signal amplification and noise reduction

Signal amplification and noise reduction are critical for successful development of ultrasensitive sandwich-type aptasensor. The signal amplification performance of the proposed aptasensor was investigated and the results were shown in Fig. 4B. The curve *b* showed the redox peak current of the aptasensor after the sandwich format reaction with 10 nM PDGF, it was found that a pair of well-defined redox wave, corresponding to the reversible redox reaction of Au@PB/$FC_{60}$. More importantly, with the addition of AA–P, the oxidation peak current of curve *c* was greatly enhanced comparing with curve *b*. The result may be attributed to the dual signal amplification process: AP on the electrode surface could catalyze hydrolysis of AA–P to in-situ produce AA which could be further catalyzed by Au@PB/$FC_{60}$ to obtain quite fast, stable and greatly amplified signal. Moreover, the non-specific fouling effect of the aptasensor was also studied by incubated with 0 nM PDGF standard solution (Fig. 4B, curve *a*). The result indicated the proposed aptasensor with the lower background noise.

### 3.5. Performance of the aptasensor

The performance of the present aptasensor was evaluated by detecting PBGF-BB standard solutions with the addition of 5.0 mM AA–P under the optimization conditions. Fig. 5A showed the typical

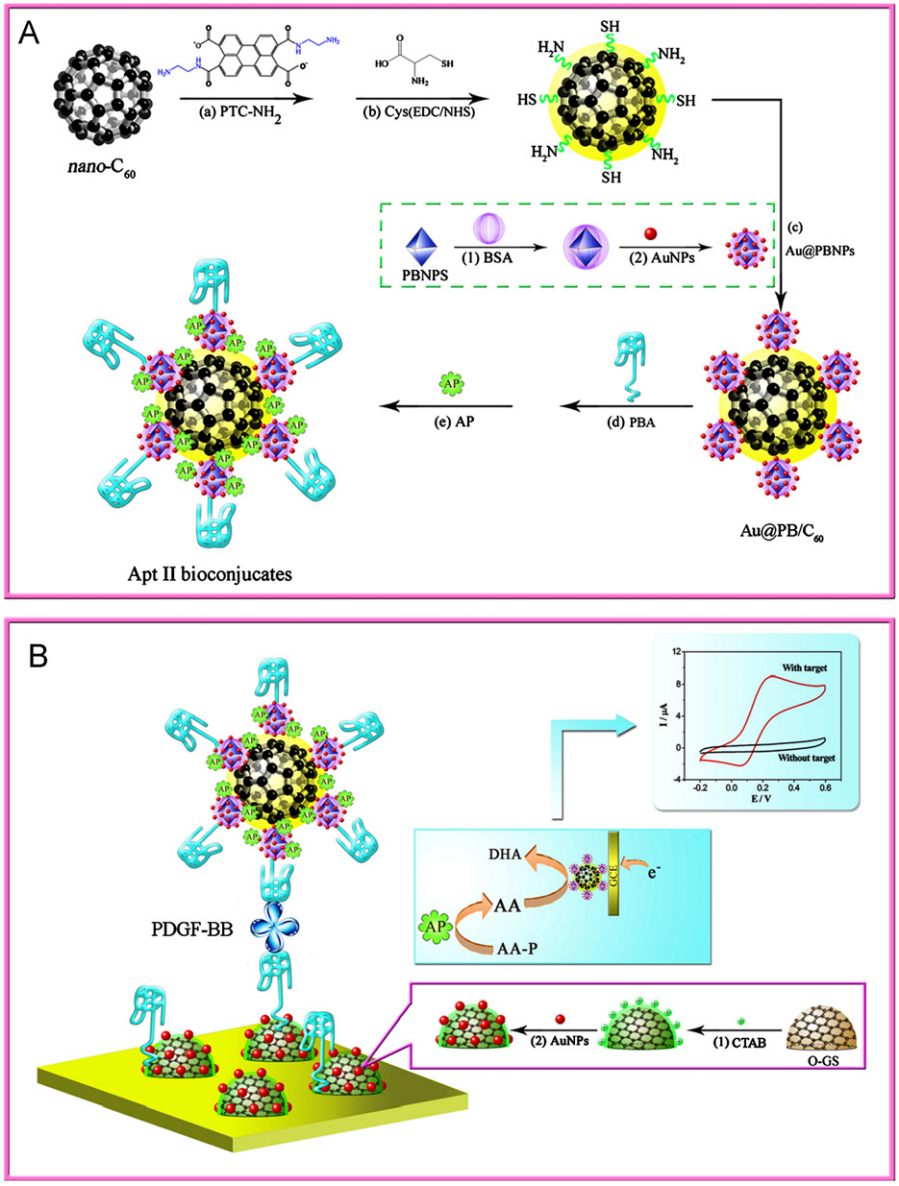


**Fig. 1.** (A) Preparation procedure of Apt II bioconjugates (AP/Apt II/Au@PB/$FC_{60}$). (B) Schematic illustration of the stepwise aptasensor fabrication process and the dual signal amplification mechanism.

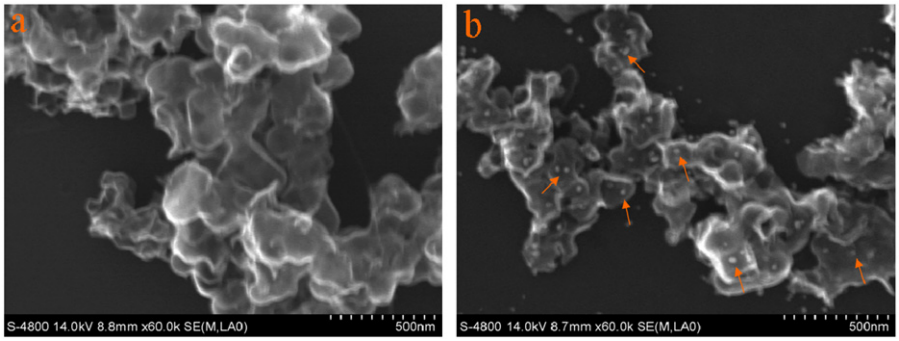


**Fig. 2.** SEM images of O-GS (a) and AuNPs/O-GS (b).

DPV obtained after the sandwich reactions for different concentrations of PBGF-BB using AP/Apt II/Au@PB/$FC_{60}$ bioconjugates as tracer. As expected, the DPV responses increased with the increment of PBGF-BB concentrations after the complementary pairing interaction. As shown in Fig. 5B, the calibration plots showed a good linear relationship between the oxidation peak currents and the analyte concentrations in the ranges from 0.002 to 40 nM with a regression equation of $y=0.599x+4.319$ (nM) and a detection limit of 0.6 pM ($S/N=3$). The higher sensitivity and wider linear range of the proposed aptasensor should be taken into account as the

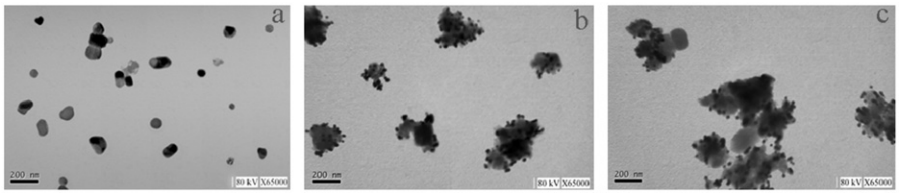


**Fig. 3.** TEM images of $FC_{60}$NPs (a), Au@PBNPs (b) and Au@PB/$FC_{60}$ (c).

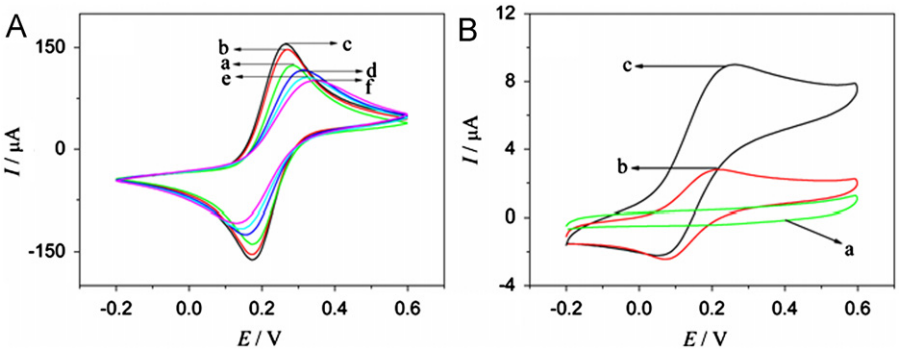


**Fig. 4.** (A) CVs of different electrodes in 5.0 mM $Fe(CN)_6^{3-/4-}$ solution containing 0.1 M KCl at a scan rate of 50 mV/s: (*a*) bare GCE, (*b*) O-GS/GCE, (*c*) AuNPs/O-GS/GCE, (*d*) Apt I/AuNPs/O-GS/GCE, (*e*) HT/Apt I/AuNPs/O-GS/GCE, (*f*) after incubated with 10 nM PDGF. (B) The CVs after the sandwich immunoreaction with 0 nM PDGF (*a*) and 10 nM PDGF (*c*) in the presence of 5.0 mM AA-P in 0.1 M PBS, and 10 nM PDGF without AA-P in 0.1 M PBS (*b*).

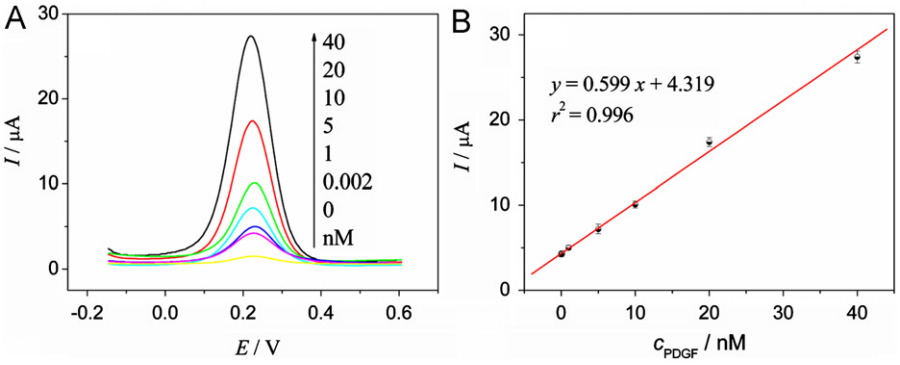


**Fig. 5.** (A) DPV responses of the proposed immunosensor after incubation with different concentration of PDGF. (B) Calibration curves for determination of PDGF using AP/Apt II/Au@PB/$FC_{60}$ bioconjugates as tracer. The error bars represent the standard deviations of three parallel samples at each target concentration.

employment of the favorable redox electrochemical activity and the high-performance amperometric response of Au@PB/$FC_{60}$ which exhibited satisfactory performance as expected.

### 3.6. Specificity, reproducibility and stability of the aptasensor

The specificity of the aptasensor played a very important role in analyzing biological samples in situ without separation. To assess the binding specificity of the proposed aptasensor to PDGF-BB, control experiments were performed by using 1 μM hemoglobin (Hb) and 1 μM BSA to replace 10 nM PDGF-BB, respectively. The evaluated results were shown in Fig. 6. It was found that the presence of the interferences exhibits no significant effect on the current intensity compared with the absence of PDGF-BB, indicating that PDGF-BB-specific aptamer sequence was quite specific to PDGF-BB. Moreover, the cross-sensitivity of the aptasensor in a mixture solution (10 nM PDGF-BB containing 1 μM Hb and 1 μM BSA) was also investigated. Although high concentration of Hb and BSA were coexisted, the detection signals had no apparent difference, implying that the above interferents had almost negligible influence for PDGF-BB detection. The experimental results demonstrated that the proposed aptasensor based on the high specific recognition had satisfying selectivity.

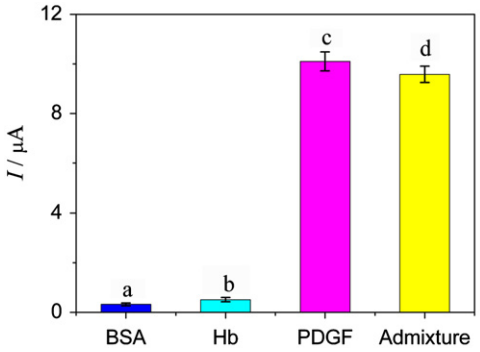


**Fig. 6.** Specificity of the immunosensor: (a) with 1 μM of BSA; (b) with 1 μM of Hb; (c) with 10 nM of PDGF; (d) with 10 nM of PDGF when 1 μM of BSA and 1 μM of Hb were coexisted(error bars: SD, $n=3$).

The reproducibility of the aptasensor was evaluated by analysis of the same concentration of 10 nM PDGF-BB with five equally prepared electrodes. All electrodes exhibited similar electrochemical responses with an acceptable relative standard deviation (RSD) of 4.79% ($n=5$).

Furthermore, the stability of the aptasensor was investigated long-term storage assay. When the rustled electrodes were not in use, they were stored at 4 °C. It can be seen that 95.2% of the initial response remained after one week and 86.7% of the initial response remained after four weeks. The results showed that the stability of aptasensor was satisfactory. Meanwhile, these results also highlighted that Au@PB/$FC_{60}$ as tracing tag had good stability and biocompatibility.

## 4. Conclusions

In conclusion, the present study demonstrated the highly sensitive electrochemical aptasensor by means of Apt II and AP labeled Au@PB/$FC_{60}$ as tracer. The sensing probes of AP/Apt II/Au@PB/$FC_{60}$ could amplify the signal by biocatalysis of AP towards AA–P to in-situ production of AA and then chemicatalysis of Au@PB/$FC_{60}$ towards AA to generate DHA. Highlights of this work can be summarized as follows: At first, $FC_{60}$NPs, which was synthesized by supramolecular interaction and amenable to biological studies, displayed the large surface active sites and good water-stability. Moreover, the Au@PB/$FC_{60}$ exhibits high electrocatalytic activity and is a promising redox probe to generate high-performance amperometric response, thus greatly enhanced the detection signal for sandwich-type assay. Significantly, the large surface area, rich active sites, low background and favorable microenvironment made the Au@PB/$FC_{60}$ may become a promising nano-material for electrochemical aptasensing applications. Finally, we expect many exciting opportunities to explore $C_{60}$-based new nanomaterials in future.

## Acknowledgements

This research was supported by the NNSF of China (21105081, 21075100, 21275119), Research Fund for the Doctoral Program of Higher Education (RFDP) (20110182120010), Ministry of Education of China (Project 708073), Specialized Research Fund for the Doctoral Program of Higher Education (20100182110015) and Natural Science Foundation Project of Chongqing City (CSTC-2010BB4121, CSTC-2011BA7003, CSTC-2009BA1003), the Fundamental Research Funds for the Central Universities (XDJK2010C062, XDJK2012A004), China.

## Appendix A. Supporting information

Supplementary data associated with this article can be found in the online version at http://dx.doi.org/10.1016/j.bios.2013.02.020.

## References

Andrievsky, G.V., Klochkov, V.K., Karyakina, E.L., Mchedlov-Petrossyan, N.O., 1999. Chemical Physics Letters 300, 392–396.
Colvin, V.L., 2003. Nature Biotechnology 21, 1166–1170.
Doolittle, R.F., Hunkapiller, M.W., Hood, L.E., Devare, S.G., Robbins, K.C., Aaronson, S.A., Antoniades, H.N., 1983. Science 221, 275–277.
D'Souza, F., Ito, O., 2009. Chemical Communications 33, 4913–4928.
Enustun, B.V., Turkevich, J., 1963. Journal of the American Chemical Society 85, 3317–3328.
Fiorito, P.A., Goncales, V.R., Ponzio, E.A., De Torresi, S.I.C, 2005. Chemical Communications 3, 366–368.
Guo, S.J., Du, Y., Yang, X., Dong, S.J., Wang, E.K., 2011. Analytical Chemistry 83, 8035–8040.
Halder, A., Nayak, S.K., Chattopadhyay, S., Bhattacharya, S., 2012. Journal of Solution Chemistry 41, 223–240.
Hilburn, M.E., Murdianti, B.S., Maples, R.D., Williams, J.S., Damron, J.T., Kuriyavar, S.I., Ausman, K.D., 2012. Colloids and Surfaces A: Physicochemical and Engineering Aspects 401, 48–53.
Huang, C.C., Huang, Y.F, Cao, Z.H, Tan, WH., Chang, H.T., 2005. Analytical Chemistry 77, 5735–5741.
Ko, W.B., Heo, J.Y., Nam, J.H., Lee, K.B., 2004. Ultrasonics 41, 727–730.
Kroto, H.W., Heath, J.R., O'Brien, S.C., Curl, R.F., Smalley, R.E., 1985. Nature 318, 162–163.
Lei, J.P., Ju, H.X., 2012. Chemical Society Reviews 41, 2122–2134.
Li, W.J., Yuan, R., Chai, Y.Q., 2010. Journal of Physical Chemistry C 114, 21397–21404.
Lin, D.J., Wu, J., Wang, M., Yan, F., Ju, H.X., 2012. Analytical Chemistry 84, 3662–3668.
Liu, S.Q., Xu, J.J., Cheng, H.Y., 2002. Electrochemistry Communications 4, 421–425.
Liu, Y., Chen, G.S., Chen, Y., Zhang, N., Chen, J., Zhao, Y.L., 2006. Nano Letters 6, 2196–2200.
Machado, B.F., Serp, P., 2012. Catalysis Science & Technology 2, 54–75.
Martín, N., 2006. Chemical Communications 20, 2093–2104.
Mashayekhi, H., Ghosh, S., Du, P., Xing, B.S., 2012. Journal of Colloid and Interface Science 374, 111–117.
Nielsen, K.A., Cho, W.S., Sarova, G.H., Petersen, B.M., Bond, A.D., Becher, J., Jensen, F., Guld, D.M., Sessler, J.L., Jeppesen, J.O., 2006. Angewandte Chemie International Edition 118, 7002–7007.
Park, S., Ruoff, RS., 2009. Nature Nanotechnology 4, 217–224.
Pereira, A.M.V.M., Hausmann, A., Tomé, J.P.C., Trukhina, O., Urbani, M., Neves, M.G.P.M.S., Cavaleiro, J.A.S., Guldi, D.M., Torres, T., 2012. Chemistry A European Journal 18, 3210–3219.
Poddutoori, P.K., Sandanayaka, A.S.D., Hasobe, T., Ito, O., Est, A., 2010. Journal of Physical Chemistry B 114, 14348–14357.
Qiu, J.D., Peng, H.Z., Liang, R.P., Li, J., Xia, X.H., 2007. Langmuir 23, 2133–2137.
Regehly, M., Ermilov, E.A., Helmreich, M., Hirsch, A., Jux, N., Röder, B., 2007. Journal of Physical Chemistry B 111, 998–1006.
Stankovich, S., Dikin, D., Dommett, G., Kohlhaas, K., Zimney, E., 2006. Nature 442, 282–286.
Xu, Y.Y., Zhua, J.D., Xiang, K., Li, Y.K., Sun, R.H., Ma, J., Sun, H.F., Liu, Y.F., 2011. Biomaterials 32, 9940–9949.
Yang, J.Z., Barron, A.R., 2004. Chemical Communications 24, 2884–2885.
Zhang, E.X., Wang, D.X., Zheng, Q.Y., Wang, M.X., 2008. Organic Letters 12, 2565–2568.
Zhong, X., Yuan, R., Chai, Y.Q., 2012. Chemical Communications 48, 597–579.
Zhou, J., Zhuang, J.Y., Miró, M., Gao, Z.Q., Chen, G.N., Tang, D.P., 2012. Biosensors and Bioelectronics 35, 394–400.
Zhuo, Y., Yuan, P.X., Yuan, R., Chai, Y.Q., Hong, C.L., 2008. Biomaterials 29, 1501–1508.
Zhuo, Y., Yuan, P.X., Yuan, R., Chai, Y., Hong, C.L., 2009. Biomaterials 30, 2284–2290.